



HAL
open science

Rational Design of Highly Efficient PdIn-In 2 O 3 Interfaces through Capture-alloying Strategy for Benzyl Alcohol Partial Oxidation

Peng Bai, Zhenxiang Zhao, Yonghui Zhang, Zhengke He, Yonghui Liu, Chunzheng Wang, Shixingwang Ma, Pingping Wu, Lianming Zhao, Svetlana Mintova, et al.

► **To cite this version:**

Peng Bai, Zhenxiang Zhao, Yonghui Zhang, Zhengke He, Yonghui Liu, et al.. Rational Design of Highly Efficient PdIn-In 2 O 3 Interfaces through Capture-alloying Strategy for Benzyl Alcohol Partial Oxidation. ACS Applied Materials & Interfaces, 2023, 15 (15), pp.19653-19664. 10.1021/acsami.3c00810 . hal-04285841

HAL Id: hal-04285841

<https://hal.science/hal-04285841>

Submitted on 14 Nov 2023

HAL is a multi-disciplinary open access archive for the deposit and dissemination of scientific research documents, whether they are published or not. The documents may come from teaching and research institutions in France or abroad, or from public or private research centers.

L'archive ouverte pluridisciplinaire **HAL**, est destinée au dépôt et à la diffusion de documents scientifiques de niveau recherche, publiés ou non, émanant des établissements d'enseignement et de recherche français ou étrangers, des laboratoires publics ou privés.

Rational Design of Highly Efficient PdIn-In₂O₃ Interfaces through Capture-alloying Strategy for Benzyl Alcohol Partial Oxidation

Peng Bai,^{†,} Zhenxiang Zhao,[†] Yonghui Zhang,[†] Zhengke He,[†] Yonghui Liu,[#] Chunzheng*

Wang,[†] Shixingwang Ma,[†] Pingping Wu,^{†,} Lianming Zhao,^{#,*} Svetlana Mintova,^{||}*

Zifeng Yan[†]

[†]State Key Laboratory of Heavy Oil Processing, CNPC Key Laboratory of Catalysis,

College of Chemistry and Chemical Engineering, China University of Petroleum

(East China), Qingdao 266580, China

[#]School of Materials Science and Engineering, Institute of Advanced Materials, China

University of Petroleum (East China), Qingdao, 266580, China

^{||}Normandie University, ENSICAEN, UNICAEN, CNRS, Laboratoire Catalyse et

Spectrochimie, 14000 Caen, France

ABSTRACT: Well-dispersed PdIn bimetallic alloy nanoparticles (1 ~ 4 nm) were immobilized on mesostructured silica through an *in situ* capture-alloying strategy and PdIn-In₂O₃ interfaces were rationally constructed by changing the In₂O₃ loading and varying the reduction temperature. The catalytic performance for benzyl alcohol partial oxidation was evaluated and a catalytic synergy was observed. The Pd-rich PdIn-In₂O₃ interface is prone to formation on the catalyst with a low In₂O₃ loading after reduced at 300 °C. It was demonstrated that the Pd-rich PdIn-In₂O₃ interface is more active for benzyl alcohol partial oxidation than In-rich Pd₂In₃ species which is likely to be formed at a high reduction temperature (400 °C). The high catalytic activity on Pd-rich PdIn-In₂O₃ interface was attributed to the exposure of more Pd-enriched active sites and an optimized PdIn-In₂O₃/Pd assemble ratio enhanced the oxygen transfer during the partial oxidation. The DFT calculation confirmed that the Pd-rich Pd₃In₁(111)-In₂O₃ interface facilitated the activation of oxygen molecules, resulting in a high catalytic activity.

KEYWORDS: PdIn, alloy nanoparticles, interface, capture-alloying strategy, partial oxidation

1. INTRODUCTION

Partial oxidation of primary alcohols to corresponding aldehydes or ketones is crucial in organic synthesis since high-value added products or fine chemical intermediates are produced^{1,2}. Among which, benzaldehyde is a very important aromatic molecule

used in the cosmetics and condiments industry. Since 1863, benzaldehyde has been synthesized through benzene chloride hydrolysis as a by-product.³ However, the presence of organic chlorine or benzoic acid in the products limits the use of benzaldehyde in food and cosmetic field. The oxidation of benzyl alcohol (BA) to benzaldehyde using oxygen gas conforms with the principles of green and sustainable chemistry and provides high quality benzaldehyde products. However, with oxygen gas as the oxidant, benzaldehyde is prone to over-oxidation, leading to decrease of selectivity of desired products. Hence, the key to the industrialization of benzyl alcohol partial oxidation process is the development of efficient catalysts with high activity and high selectivity to useful products.⁴

Supported noble metal nanoparticles (NPs) catalysts such as Pd,^{5, 6} Pt,⁷ Au⁸ have been investigated in catalytic oxidation and hydrogenation reactions. Recently, supported Pd NPs catalysts attracted the attention of researchers dealing with partial oxidation reactions.^{9, 10} Metallic Pd⁰-enriched clusters/surface has been widely accepted as active sites for oxidation reactions,¹¹⁻¹⁶ however, it is unavoidable to form an inert PdO layer on Pd⁰-enriched Pd surface.^{17, 18} This problem has been reported in several papers and the formation of PdO layer was possible to be retarded by introducing promoters to Pd.^{10, 14} In our previous work, Au and Sn have been added to Pd NPs as promoters to inhibit the formation of PdO.^{14, 19} The results demonstrated that alloying of Au-Pd partially prevent the easy oxidation of surface Pd atoms after H₂ reduction. The *in situ* reduction of surface PdO layer was achieved by the addition

of Sn species to Au-Pd alloy NPs instead of high temperature H₂ reduction treatment.¹⁹

For partial oxidation reaction, the key towards enhancement of catalyst activity is the improvement of adsorption and activation of reactants^{14, 20, 21} and oxygen transfer capacity of catalysts.^{22, 23} Among them, Pd based catalysts show high activity in the process of partial oxidation reaction since the d band of Pd partially overlaps with the Fermi level leading to strong adsorption capacity for reactants.²⁴ The addition of promoter modifies the activity of the catalyst through the ligand^{25, 26} and structural effects.^{27, 28} The activation sites for O₂ on Pd based catalyst is at the interface between active component and support²⁹ or between active component and promoter¹⁴ have been reported. In our previous work, bimetallic (Au-Pd)-oxide (SnO_x) interfaces have been constructed for benzyl alcohol partial oxidation.¹⁹ The Pd-enriched Au-Pd alloy sites were found to be responsible for O₂ activation and the adjacent SnO_x sites promoted the O transfer, leading to a high catalytic activity. However, after H₂ reduction, the SnO_x was partially reduced and Au-Pd-Sn alloy was generated with the loss of AuPd/SnO_x interfaces, which dramatically decreased the catalyst activity.¹⁹ These findings suggest that more efforts are needed to explore efficient promoters and construct active metal (bimetal)-oxide interfaces for the partial oxidation reaction.

Indium or In₂O₃ have recently emerged as a promising promoter for Pd based catalysts to enhance the catalytic performance for ethane dehydrogenation,³⁰ CO₂-selective methanol steam reforming³¹ and CO₂ hydrogenation to methanol.^{32, 33} The formation of intermetallic PdIn species alone was shown not to be sufficient to

achieve the catalytic synergy of PdIn bimetallic catalyst; the presence of oxidized indium surface was essential. Thus, the presence of PdIn bimetal/oxide interface is considered to be the key for the catalytic synergy between PdIn intermetallic compound and indium oxide.^{2, 31} This implies that the PdIn-In₂O₃ interface may be also active in the partial oxidation of benzyl alcohol. The problem in constructing PdIn bimetal-oxide interface is the aggregation of Pd and/or In species resulting in nanoparticles with size from 20 nm to 50 nm using the traditional impregnation method^{33, 34} that reduce substantially the active interfaces. Therefore, the development of a strategy to construct well-dispersed NPs catalysts with abundant PdIn-In₂O₃ interfaces for benzyl alcohol partial oxidation is highly desired.

In this work, well-dispersed Pd NPs were immobilized in mesostructured cellular foam (MCF) silica through a one-pot synthesis with mercaptopropyltrimethoxysilane (MPTMS) as an anchoring ligand, while indium was introduced through a wet impregnation procedure. Since In₂O₃ particles have a high tendency to become mobile and aggregate during heating, immobilized Pd NPs may act as a capturing agent through the formation of PdIn alloys during the reduction process, preventing the aggregation and loss of Pd and/or In₂O₃ species. An optimized PdIn-In₂O₃ interface with defined Pd/In and PdIn/In₂O₃ ratios in the alloy was achieved through changing the In₂O₃ loading and the reduction temperature. The catalytic performance of catalysts was evaluated and a catalytic synergy was observed. The detailed structure of the active sites and the mechanism of the catalytic synergy for partial oxidation were clarified.

2. EXPERIMENTAL SECTION

2.1. Chemicals. PdCl₂ (Sinopharm Chemical), In(NO₃)₃·H₂O (Sinopharm Chemical), tetraethyl orthosilicate (TEOS, 98%, Sinopharm Chemical), triblock co-polymer PEO₂₀PPO₇₀PEO₂₀ (P123, Aldrich), mercaptopropyltrimethoxysilane (MPTMS, 97%, Aldrich), 1, 3, 5-trimethylbenzene (99%, Sinopharm Chemical), hydrochloric acid (37%, Sinopharm Chemical), benzyl alcohol (99.99%, Sinopharm Chemical), benzaldehyde (99.99%, Sinopharm Chemical), benzoic acid (99.99%, Sinopharm Chemical) and absolute ethanol (99.98%, Sinopharm Chemical) were used as received without further purification.

2.2. Preparation of $y\text{In}_2\text{O}_3@\text{Pd}/\text{MCF-T-H}_2$ Catalysts. Pd/MCF was prepared following the same procedure as reported previously¹⁴ with a Pd weight loading of 0.5wt.%. For the loading of In₂O₃, 2 g of Pd/MCF precursor was dispersed in a certain amount of indium nitrate solution, followed by stirring at room temperature for 12 hours until a slurry was formed. Then the mixture was dried at 100 °C for 12 hours, and finally calcined at 400 °C for 3 hours. The obtained catalysts were denominated as $y\text{In}_2\text{O}_3@\text{Pd}/\text{MCF-ox}$ (y represents the weight percentage of In₂O₃, and ox represents the oxidation state of catalyst before H₂ reduction). The obtained catalysts were reduced in hydrogen atmosphere for 2 hours, and the catalysts reduced under different temperatures were denominated as $y\text{In}_2\text{O}_3@\text{Pd}/\text{MCF-T-H}_2$, T= 250, 300, 350, 400 °C, respectively. A reference sample 1.0%In₂O₃/MCF-ox was synthesized too. Catalysts 0.5%In₂O₃@ 1.0%Pd/MCF-300-H₂, 1.0%In₂O₃@1.0%Pd/MCF-300-H₂

and 2.0%In₂O₃@1.0%Pd/MCF-300-H₂ with high Pd (1.0wt.%) loading were prepared and subjected to further analysis.

Catalyst 0.5%In₂O₃@Pd/MCF-im was prepared by a stepwise wet impregnation method and used as a reference. In a typical synthesis, 1 g of MCF was dispersed in 10 mL of PdCl₂ solution and stirred at room temperature for 12 hours until a slurry was formed. The slurry was further dried at 100 °C overnight and then calcined at 400 °C for 3 h to obtain sample Pd/MCF-im. In₂O₃ was introduced following the same procedure as Pd. The obtained catalysts were reduced at 300 °C under hydrogen atmosphere for 2 hours and the obtained catalysts was denominated as 0.5%In₂O₃@Pd/MCF-im. Loadings of both Pd and In were 0.5wt.%.

2.3 Characterization of Catalysts. N₂ adsorption/desorption was carried out to analyze the textural properties of catalysts after degassing at 300 °C for 4 h under vacuum using an automatic volumetric sorption analyzer (Micromeritics, TriStar 3000). The surface area was calculated by the Brunauer-Emmett-Teller (BET) method. The total pore volume was calculated at $P/P_o = 0.998$. The pore diameter was calculated from the adsorption branch using the Barrett-Joyner-Halenda (BJH) method.

High angle annular dark field (HAADF) images and X-ray energy dispersive spectra (XEDS) of the catalysts were obtained using a scanning transmission electron microscope (STEM) (JEOL JEM-2100F) with an acceleration voltage of 200 kV.

X-ray powder diffraction (XRD) patterns of catalysts were recorded on a X'Pert PRO MPD system with a Cu *K* α radiation ($\lambda = 0.15418$ nm) at 35 kV and 40 mA.

Actual metal loadings in the catalysts were determined by inductively coupled plasma - optical emission spectroscopy (ICP-OES) using a VISTA-MPX Varian system. The solid ultraviolet-visible (UV-vis) spectra of catalysts were collected from a Hitachi U-4100 UV-vis-NIR spectrophotometer using BaSO₄ as an internal reference. The diffusion reflectance spectra from 350 to 800 nm were recorded.

The surface chemical properties of the catalysts were analyzed using a K-Alpha X-ray spectrometer (XPS) manufactured by Thermo Fisher Scientific. Taking the Al electrode as the anode, the electron kinetic energy is 1486.6 eV. The spectra were calibrated with C1s binding energy (284.5 eV) as a calibration binding energy (BE) reference.

In situ diffuse reflectance infrared Fourier transform (DRIFT) spectra of CO adsorption on the fresh catalysts were recorded on a BRUKER VERTEX70V FT-IR spectrometer at room temperature with a resolution of 4 cm⁻¹. The analysis was conducted in a high temperature diffuse reflection reaction cell (PIKE). The catalyst was pretreated in H₂ at 623 K with a flow rate of 20 mL min⁻¹ for 60 min, followed by cooling down to 303 K and purging with He for 30 min.

The synchrotron radiation experiments were performed at the BL14B1 of SPring-8 (8 GeV, 100 mA), Japan, to obtain X-ray adsorption fine structure (XAFS) spectra both in near and extended edge. The samples were filled in a phi10 stainless tube. Pd foil and PdO powder samples were used as references and all samples were measured in the transmission mode. Data were normalized using the Athena program with a linear pre-edge and polynomial post-edge background subtracted from the raw data.³⁵

EXAFS fits were performed using ARTEMIS software.³⁶ The interatomic distances were optimized by fitting the experimental data.

2.4 Catalytic Test: Selective Oxidation of Benzyl Alcohol. The partial oxidation of benzyl alcohol was carried out in a 100 mL autoclave with a polytetrafluoroethylene liner (Model: SLM100, Beijing Easychem Science and Technology Development Company, China). Typically, 10.8 g of benzyl alcohol and 50 mg of solid catalyst were charged into the reactor. After purging with O₂ for 3 times, the temperature was raised to 110 °C and the O₂ pressure was maintained at 0.8 MPa for 1 h under stirring. After reaction, the products were separated and analyzed using a gas chromatogram (Agilent 6870) equipped with a flame ionization detector (FID) and a DB-1 column (30*0.32*0.25). The turnover frequency (TOF) was calculated based on the moles of benzyl alcohol converted per mole of Pd per hour. The standard deviations were calculated based on three repeated experiments.

2.5 Density Functional Theory Calculations. The spin-polarized density functional theory (DFT) calculations were conducted using the DMol³ program of Materials Studio 2018 software package.^{37, 38} The exchange-correlation term was evaluated within the general gradient approximation developed by Perdew, Burke, and Ernzerhof (GGA-PBE).³⁹ The long-range dispersion forces was established by the Grimme's PBE+D2 method,⁴⁰ revealing a comparable reliability with the PBE0 hybrid XC functional including an ab initio Van der Waals correction.⁴¹ The density functional semicore pseudopotential (DSPP) was used to model the ion cores of metal atoms, while the localized double-numerical basis with polarization (DNP) function is

applied as the valence electron functions. The linear synchronous transition/quadratic synchronous transit method was used to establish the transition state structures,⁴² which was verified by the frequency calculations. A real-space global orbital cutoff of 4.9 Å was applied to maintain the balance between high quality of results and high computational cost. The convergence tolerances for energy change, max force, and displacement were 1×10^{-5} Ha, 2×10^{-3} Ha Å⁻¹, and 5×10^{-3} Å, respectively.

The adsorption energy (E_{ads}) of an adsorbate on catalyst surfaces was defined as

$$E_{\text{ads}} = E_{\text{adsorbate/substrate}} - (E_{\text{adsorbate}} + E_{\text{substrate}})$$

where $E_{\text{adsorbate/substrate}}$ and $E_{\text{substrate}}$ correspond to the total energy of the catalyst substrate with and without an adsorbed molecule, respectively, while $E_{\text{adsorbate}}$ represents the energy of the free adsorbate.

3. RESULTS AND DISCUSSION

3.1 Catalytic Performance. The effect of reduction temperature on the catalytic performance was investigated by reduction of catalyst 0.5%In₂O₃@Pd/MCF-ox under different temperatures (250, 300, 350, 400 °C). The results are shown in Figure 1A; the detailed results from the catalytic tests are summarized in Table S1. The 0.5%In₂O₃@Pd/MCF-ox catalyst exhibited a lower catalytic activity (TOF=11872 h⁻¹) and lower benzaldehyde selectivity than those of reduced catalysts. Catalyst 0.5%In₂O₃@Pd/MCF-ox was further reduced in H₂ atmosphere at 250 °C, 300 °C, 350 °C and 400 °C, respectively. After H₂ reduction, the catalytic activity increased with the reduction temperature and the highest catalytic activity and the highest benzaldehyde selectivity were obtained on catalyst 0.5%In₂O₃@Pd/MCF-300-H₂

reduced at 300 °C in H₂. Further increasing the reduction temperature (>300 °C) led to the decrease of catalytic activity, but no obvious change in benzaldehyde selectivity was observed. This is due to the fact that the reduction of catalyst results in the formation of more surface-active sites for partial oxidation, however, the catalyst reduction above 350 °C probably led to the reconstruction of nanoparticle surface sites, thus resulting in the decreased catalytic activity. Based on above results, 300 °C was considered as the optimal reduction temperature and the variation of catalyst surface properties under different reduction temperatures will be further discussed.

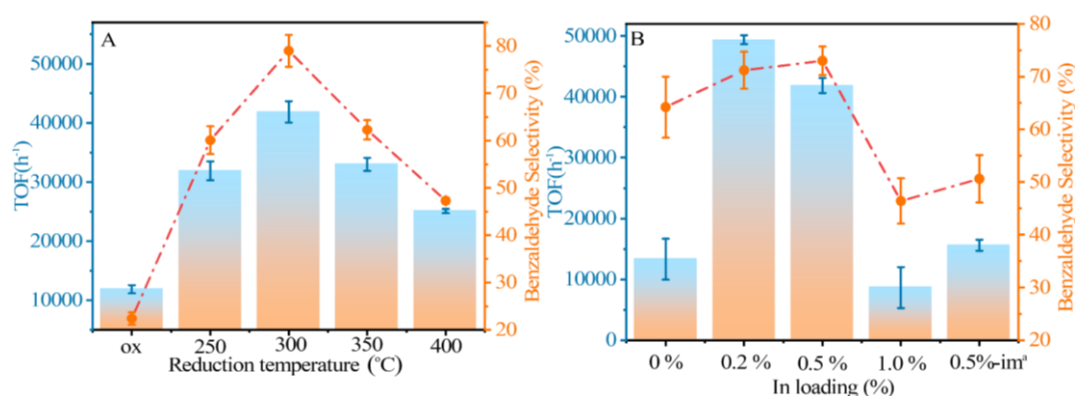


Figure 1. Catalytic performance of catalysts: (A) 0.5%In₂O₃@Pd/MCF-T-H₂ reduced at different temperatures and (B) yIn₂O₃@Pd/300°C-H₂ Catalysts with different In loadings. (a: 0.5%-im represents catalyst 0.5%In₂O₃@Pd/MCF-im which was prepared for comparison by stepwise wet impregnation method).

Catalysts with different In/Pd ratios reduced at 300 °C in H₂ atmosphere were applied for benzyl alcohol oxidation, and the results are shown in Figure 1B; the detailed results from the catalytic tests are summarized in Table S2. A low benzyl alcohol conversion (25.1%) with a benzaldehyde selectivity of 64.2% on pure Pd

catalyst Pd/MCF-300°C-H₂ was obtained. After introducing the In promoter, the benzyl alcohol conversion increased dramatically to 93.2% and 79% on catalyst 0.2%In₂O₃@Pd/MCF-300-H₂ and 0.5%In₂O₃@Pd/MCF-300-H₂, respectively, with a benzaldehyde selectivity higher than 70%. When the In content increased further, the benzyl alcohol conversion decreased to 16.3% on catalyst 1.0%In₂O₃@Pd/MCF-300-H₂ with a relative low benzaldehyde selectivity (46.4%). For comparison, catalyst 0.5%In₂O₃@Pd/MCF -im prepared by wet impregnation method and reduced at 300 °C in H₂ atmosphere was evaluated too. Under the same reaction conditions, a low benzyl alcohol conversion (30.2%) with a low benzaldehyde selectivity (50.6%) on the 0.5%In₂O₃@Pd/MCF-im catalyst was obtained. These results suggested an obvious promoter effect of In species to Pd for benzyl alcohol oxidation. The capture-alloying strategy is more effective to prepare catalysts with high activity in comparison with the wet-impregnation method. Thus, the structure-performance relationship by extensively characterizing the surface and interface properties of PdIn catalysts is highly interesting to be studied.

3.2 Nature of active sites. The textural properties of catalysts were analyzed by N₂ physisorption technique, and the textural properties are summarized in Table 2. The N₂ sorption isotherms and pore size distribution curves of the catalysts are presented in Figure S1A-S1B. A typical type IV isotherms with a type H-2 hysteresis loop were measured for all catalysts, indicating the mesoporous structure of catalysts. A high specific surface area (~ 600 m²/g) was measured for most catalysts (Table 2) with an average pore size of 3.9 nm; a slight decrease of the specific surface area with the

increase of In content was detected. Higher reduction temperature (400 °C) led to lower specific surface area (535.2 m²/g) on catalyst 0.5%In₂O₃@Pd/MCF-400-H₂ than that of catalyst 0.5%In₂O₃@Pd/MCF-300-H₂ (599.4 m²/g), which is probably due to the partial contraction of pore structure of silica support. The metal loadings were measured by ICP-OES, which were found to be close to the nominal contents. XRD patterns of catalysts with different In₂O₃ contents are shown in FigureS1C. No diffraction peaks expected for In, Pd or PdIn were detected due to the low loading content and high dispersion of metals on the catalyst surface. To identify the peak positions of Pd/In on different catalysts, the 0.5%In₂O₃@1%Pd/MCF-300-H₂, 1.0%In₂O₃@ 1.0%Pd/MCF-300H₂ and 2.0%In₂O₃@1.0%Pd/MCF-300-H₂ with high metal loadings were prepared. As shown in Figure 2A, a wide diffraction peak in the 2θ range of 39 - 40° was present in the XRD patterns of samples 0.5%In₂O₃@1%Pd/MCF-300-H₂, 1.0%In₂O₃@1.0%Pd /MCF-300-H₂ and 2.0%In₂O₃@1.0%Pd/MCF -300-H₂; the peaks intensity corresponding to Pd (40.2°) and/or PdIn (39.7°) increased with increasing the content of In species due to the formation of intermetallic structure.³³ No obvious diffraction peaks of In or In₂O₃ were detected on these catalysts, indicating that Pd/PdIn alloy may be present as dominate species on catalysts yIn₂O₃@Pd/MCF-300-H₂. To further identify the specie, the catalyst 2.0%In₂O₃@1.0%Pd/MCF-300-H₂ was reduced at 400 °C and 500 °C (Figure 2B). A slight enhancement of the diffraction peak at 39.2° 2θ was observed with the increase of reduction temperature, indicating that more In atoms were incorporated into Pd phase, and PdIn intermetallic compounds may be produced.

Table 2. Properties of Catalysts

Catalysts	Metal loading ^a (wt.%)		Pd: In molar ratio	S_{BET} (m^2/g)	V_{total} (cm^3/g)	Pore diameter (nm)
	Pd	In				
Pd/MCF-300-H ₂	0.42	0	-	609.2	0.48	5.69
0.2%In ₂ O ₃ @Pd/MCF-300-H ₂	0.41	0.18	2.9:1	624.1	0.45	5.71
0.5%In ₂ O ₃ @Pd/MCF-300-H ₂	0.40	0.38	1.1:1	599.4	0.49	6.50
1.0%In ₂ O ₃ @Pd/MCF-300-H ₂	0.42	0.87	0.52:1	582.5	0.49	6.67
0.5%In ₂ O ₃ @Pd/MCF-400-H ₂	0.41	0.37	1.2:1	535.2	0.51	5.65
0.5%In ₂ O ₃ @Pd/MCF-im	0.45	0.48	1.0:1	569.0	0.98	9.82

^a The metal loading measured by ICP-OES. S_{BET} , surface area calculated by the BET method.

V_{total} , total pore volume calculated at $P/P_o = 0.998$. Pore diameter calculated from the adsorption branch using the BJH method.

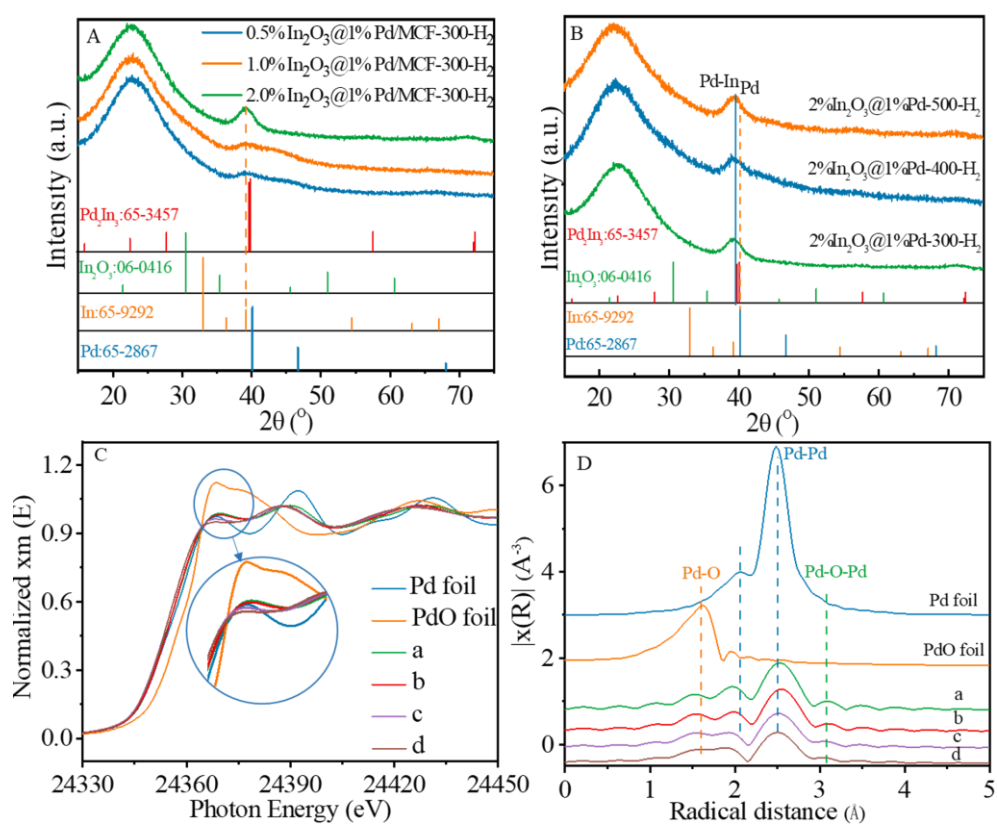


Figure 2. XRD patterns of catalysts (A-B), normalized XANES spectra (C) and Fourier transform EXAFS spectra of Pd K-edge of the monometallic and intermetallic catalysts along with the reference metal foil (Pd foil) and PdO foil (D): (a) Pd/MCF-300-H₂, (b) 0.2%In₂O₃@Pd/MCF-300-H₂, (c) 0.5%In₂O₃@Pd/MCF-300-H₂, and (d) 1.0%In₂O₃@Pd/MCF-300-H₂.

Normalized X-ray absorption near edge structure (XANES) and Fourier transform Pd K-edge EXAFS spectra of catalysts are shown in Figure 2C. In the near edge spectra of X-ray absorption, the catalysts y In₂O₃@Pd/MCF-300-H₂ exhibit similar K-edge energy (24350 eV) and white line intensity to those of Pd foil, but obviously different from the PdO foil, indicating that Pd⁰ are the dominant species on these catalysts. After the addition of In, the XANES profiles of bimetallic catalysts y In₂O₃@Pd/MCF-300-H₂ are different from that of the Pd standard. With the increase of the In content, a slight decrease of white line intensity was observed, indicating the presence of metallic In around Pd atoms³⁰ and electron transfer from In species to Pd. These results suggested the incorporation of indium into the Pd; these findings are consistent with previous results reporting on the formation of PdIn bimetallic alloy NPs.^{30, 43}

The Fourier transform EXAFS spectra of catalysts are shown in Figure 2D and the fitting parameters are summarized in Table 3. The Pd-O and Pd-Pd path intensity decreased with the increase of In content, suggesting the incorporation of In into Pd phase. The Pd-Pd bonds at 2.50 Å and 2.05 Å, Pd-O bond at 1.58 Å are determined according to the standard samples of Pd and PdO foils (Figure 2D). The Pd-Pd bond

at 2.50 Å shifts to higher value after introducing In on catalysts $y\text{In}_2\text{O}_3@\text{Pd}/\text{MCF-300-H}_2$, while that at 2.05 Å shifts to lower value with the increase of In content, suggesting the formation of PdIn alloy on the first coordination shell.³⁰ The coordination number (CN) of Pd-O on PdO foil is 4, while it decreases to 1 or less than 1 on catalysts $y\text{In}_2\text{O}_3@\text{Pd}/\text{MCF-300-H}_2$ (Table 3). Moreover, the Pd-O bond distance increases dramatically, indicating that most PdO species have been reduced to Pd⁰. The fitting data show that the CN of Pd-M on catalyst Pd/MCF-300-H₂ is 5.3 and the atomic spacing (R) is 2.738 Å, while the CN is 5.6 and R is 2.759 Å on catalyst 0.2%In₂O₃@Pd/MCF-300-H₂ after introducing In. This distance falls between that of metallic Pd (2.739 Å) and bimetallic InPd (2.81 Å) species,⁴³ which indicates the presence of Pd-Pd/Pd-In coordination in these catalysts.

Table 3. Fitting Parameters of Fourier Transform Pd K-edge EXAFS Spectra

Sample	Path	CN	R (Å)	R-factor
Pd foil	Pd-Pd	12.0	2.739	0.005
PdO	Pd-O	4.0	2.026	0.021
Pd/MCF-300-H ₂	Pd-O	1.1	2.077	0.001
	Pd-Pd	5.3	2.738	-
0.2%In ₂ O ₃ @Pd/MCF-300-H ₂	Pd-O	1.0	2.052	0.002
	Pd-M	5.6	2.759	-
0.5%In ₂ O ₃ @Pd/MCF-300-H ₂	Pd-O	0.7	2.051	0.008
	Pd-M	5.8	2.752	-
1.0%In ₂ O ₃ @Pd/MCF-300-H ₂	Pd-O	0.9	2.093	-
	Pd-M	5.2	2.747	-

The STEM-HAADF images and the corresponding EDS spectra of catalysts 0.5%In₂O₃@Pd/MCF-ox, 0.5%In₂O₃@Pd/MCF-300-H₂ and 0.5%In₂O₃@Pd/MCF-400-H₂ are presented in Figure 3 and Figure S2. Well-dispersed metal NPs are observed on all samples with the particle size in the range of 1-5 nm. The energy dispersive line scan across NPs using the In-L (red line) and Pd-L (green

line) X-rays on different catalysts were conducted to obtain the information of In and Pd distribution.⁴⁴

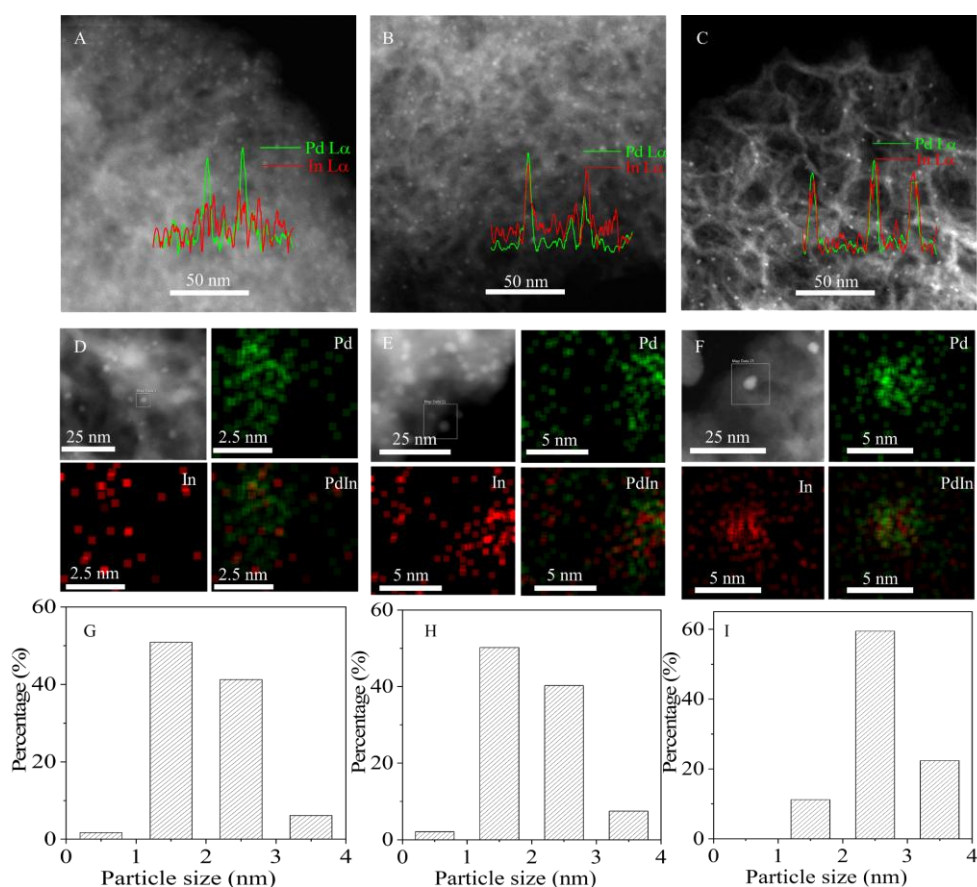


Figure 3. STEM-HAADF images of catalysts (Inset: the energy dispersive line scan across NPs using the In-L and Pd-L X-rays), corresponding color-coded EDS mapping and particle size distribution histogram of bimetallic nanoparticles on catalysts (A, D, G) $0.5\% \text{In}_2\text{O}_3 @ \text{Pd} / \text{MCF-ox}$, (B, E, H) $0.5\% \text{In}_2\text{O}_3 @ \text{Pd} / \text{MCF-300-H}_2$ and (C, F, I) $0.5\% \text{In}_2\text{O}_3 @ \text{Pd} / \text{MCF-400-H}_2$.

As shown in Figure 3A, the inset particle line scan results indicate that In is mainly distributed on the surface of the $0.5\% \text{In}_2\text{O}_3 @ \text{Pd} / \text{MCF-ox}$ catalyst. Both the EDS mapping and elemental analysis results suggested that In was mobile during the H_2 reduction process, resulting in the accumulation of In on Pd NPs (Figure 3B-C).

Figure S2 shows the STEM-HAADF images, color-coded EDS mapping and

elemental analysis of more representative bimetal nanoparticles on catalysts $0.5\% \text{In}_2\text{O}_3 @ \text{Pd/MCF-ox}$, $0.5\% \text{In}_2\text{O}_3 @ \text{Pd/MCF-300-H}_2$ and $0.5\% \text{In}_2\text{O}_3 @ \text{Pd/MCF-400-H}_2$ and the In/Pd ratio calculated from EDS elemental analysis presented in Figure S3 further confirmed the accumulation of In on Pd NPs during H_2 reduction. As is shown in Figure S2 and Figure S3, the In/Pd ratio was estimated to be 1/6 on unreduced catalyst $0.5\% \text{In}_2\text{O}_3 @ \text{Pd/MCF-ox}$ based on EDS elemental analysis of represented NPs. The In/Pd ratio increased to 1/4~1/3 on catalyst $0.5\% \text{In}_2\text{O}_3 @ \text{Pd/MCF-300-H}_2$ and to 1/2~1/1 on catalyst $0.5\% \text{In}_2\text{O}_3 @ \text{Pd/MCF-400-H}_2$ after reduction in H_2 atmosphere. With increasing the reduction temperature, the alloying degree of PdIn NPs was enhanced, as indicated by inset particle line scan results. In is mainly dispersed on the surface of catalyst $0.5\% \text{In}_2\text{O}_3 @ \text{Pd/MCF-ox}$, and Pd-rich NPs are formed. After reduction by hydrogen, the indium oxide started to be reduced and accumulated on the surface of Pd NPs forming PdIn intermetallic species on the $0.5\% \text{In}_2\text{O}_3 @ \text{Pd/MCF-300-H}_2$ catalyst. Moreover, further increasing the reduction temperature led to the formation of In-rich bimetallic NPs (catalyst $0.5\% \text{In}_2\text{O}_3 @ \text{Pd/MCF-400-H}_2$). The incorporation of In to Pd was also verified by HRTEM characterization shown in Figure S4. The change of lattice spacing revealed the transformation of Pd-rich bimetallic NPs to In-rich PdIn alloy NPs with the increase of reduction temperature. The low catalytic activity of catalyst $0.5\% \text{In}_2\text{O}_3 @ \text{Pd/MCF-400-H}_2$ is probably due to the formation of In-rich bimetallic NPs that requires further clarified.

For comparison, the characterization of the reference sample 0.5%In₂O₃@Pd/MCF-im prepared by stepwise wet impregnation by STEM-HAADF image, EDS mapping, elemental analysis and particle size distribution histogram are shown in Figure S4. A broad distribution of bimetallic NPs in the range of 1-14 nm was observed, suggesting the aggregation of Pd and In on the wet-impregnated sample. The EDS results indicated the formation of homogeneous PdIn alloy NPs as shown in Figure S4 thus revealing the easy alloying of Pd with In. While well-dispersed metal NPs (1-4 nm) were obtained on catalyst 0.5%In₂O₃@Pd/MCF-300-H₂ prepared with similar metals (Pd and In) loading under the same reduction conditions. The only difference is the introduction procedure of Pd on the two catalysts. Pd was immobilized in silica support by one-pot procedure on catalyst 0.5%In₂O₃@Pd/MCF-300-H₂, while a wet impregnation method was applied to load Pd on catalyst 0.5%In₂O₃@Pd/MCF-im. Well dispersed PdIn alloy NPs were obtained through capturing In by immobilized Pd during the reduction of catalyst 0.5%In₂O₃@Pd/MCF-300-H₂. However, alloying and aggregation of Pd and In occurred on catalyst 0.5%In₂O₃@Pd/MCF-im during the reduction process. These results suggested that the *in-situ* capture-alloying strategy is effective for the preparation of well dispersed PdIn alloy NPs (1-4 nm) catalyst. And the low catalytic activity of catalyst 0.5%In₂O₃@Pd/MCF-im may be partially attributed to the poor dispersion of metal NPs.

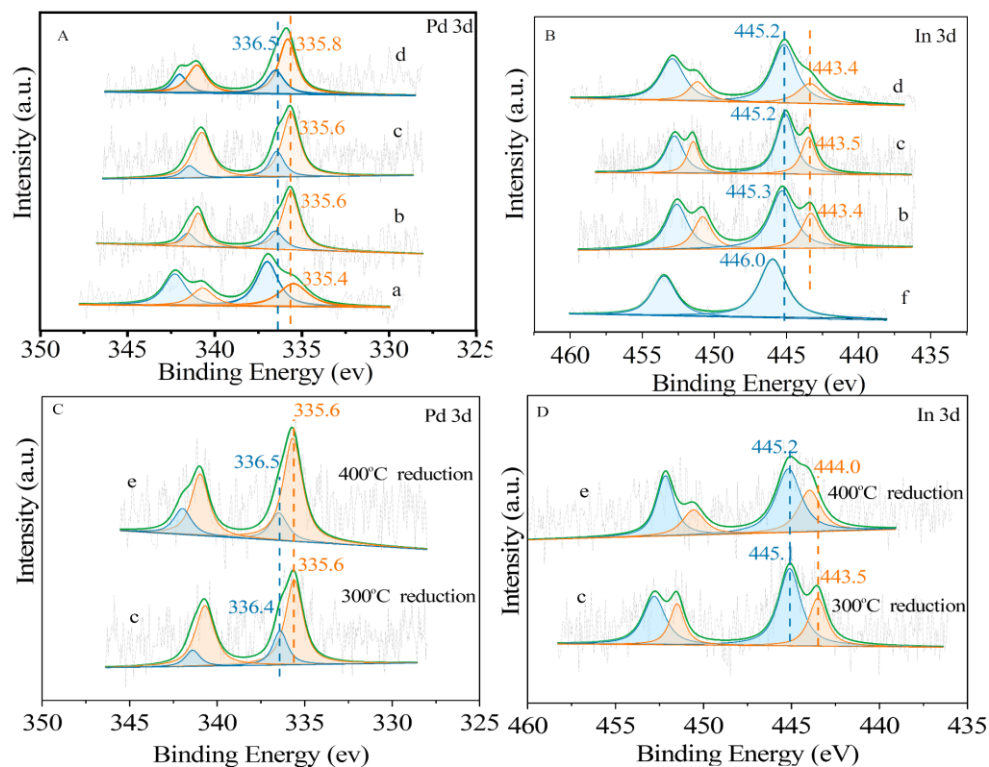


Figure 4. Pd 3d (A, C) and In 3d XPS spectra (B, D) of catalysts: (a) Pd/MCF-300-H₂, (b) 0.2%In₂O₃@Pd/MCF-300-H₂, (c) 0.5%In₂O₃@Pd/MCF-300-H₂, (d) 1.0%In₂O₃@Pd/MCF-300-H₂, (e) 0.5%In₂O₃@Pd/MCF-400-H₂ and (f) In100/MCF-300-H₂.

Table 4. Binding Energies of In and Pd Elements at Different Atomic Ratios of In/Pd, Pd/PdO and In₂O₃/In

Catalyst	BE 3d _{5/2} (eV)		Ratio			
	Pd ⁰ (Pd ²⁺)	In ⁰ (In ³⁺)	ICP In/Pd	XPS In/Pd	Pd: PdO	In: In ₂ O ₃
Pd/MCF-300-H ₂	335.4(337.0)	---	---	---	0.7:1	----
0.2%In ₂ O ₃ @Pd/MCF-300-H ₂	335.6(336.5)	443.4(445.3)	0.4:1	2.0:1	3.2:1	0.45:1
0.5%In ₂ O ₃ @Pd/MCF-300-H ₂	335.6(336.5)	443.5(445.2)	1:1	1.4:1	3.0:1	0.50:1
1.0%In ₂ O ₃ @Pd/MCF-300-H ₂	335.8(336.5)	443.4(445.2)	2:1	3.8:1	2.3:1	0.34:1
1.0%In ₂ O ₃ /MCF-300-H ₂	---	446.0	---	---	----	0:1
0.5%In ₂ O ₃ @Pd/MCF-400-H ₂	335.6(336.5)	444.0(445.2)	1:1	1.2:1	4.0:1	0.6:1

The surface composition and valence states of catalysts were characterized by XPS. The XPS spectra of Pd 3d and In 3d are shown in Figure 4 and the detailed binding energies/atom ratios are summarized in Table 4. As shown in Figure 4A, the spectra of Pd 3d were fitted by two doublets on all catalysts, and the Pd $3d_{5/2}$ with binding energy of 337.0 eV was attributed to the presence of Pd²⁺ (~ 337.2 eV)^{45, 46} and the energy value of 335.4 eV was ascribed to metallic Pd⁰ (~ 335.5 eV).^{47, 48} The Pd/PdO ratio increases dramatically with the introduction of In species, from 0.7/1 for Pd/MCF-300-H₂ to 3.2/1 for 0.2%In₂O₃@Pd/MCF-300-H₂, 3.0/1 and 0.5%In₂O₃@Pd/MCF-300-H₂, and 2.3/1 for 1.0%In₂O₃@Pd/MCF-300-H₂ catalysts. The presence of oxidized Pd²⁺ in the reduced Pd/MCF-300-H₂ catalyst is due to the easy oxidation of surface Pd⁰ to PdO in air or humid atmosphere at room temperature,⁴⁹ while introducing In species prevented the oxidation of surface Pd⁰, which is probably due to the formation of surface PdIn intermetallic structure (see XRD results in Figure 2A-2B). These statements required further clarification. The spectra of In 3d are shown in Figure 4B, and only In³⁺ with BE of 446.0 eV⁵⁰ was observed on catalyst 1.0%In₂O₃/MCF-300-H₂ since the supported indium oxide starts to be reduced at above 500 °C.⁵¹ However, two doublets on catalysts *y*In₂O₃@Pd/MCF-300-H₂ were observed, indicating the presence of both In³⁺ (~ 445.2 eV) and In⁰ (~ 443.4 eV) species. These results demonstrated that Pd also promoted the partially reduction of In³⁺ to In⁰ at 300 °C in H₂ atmosphere and probably resulted in the formation of PdIn intermetallic structure (Pd + H₂ + In₂O₃ → PdIn + H₂O).⁵² The bulk (ICP) and surface (XPS) In/Pd ratios are presented in Table

4. The results suggested that In was accumulated on the surface of catalysts. Moreover, the surface In/In₂O₃ ratio in the range of 0.34/1 ~ 0.5/1 was measured for yIn₂O₃@Pd/MCF-300-H₂ catalysts, which indicate the formation of PdIn-In₂O₃ interfaces. The coverage of Pd NPs was closely related to In content. The catalyst 0.5%In₂O₃@Pd/MCF-400-H₂ reduced at 400 °C exhibits a lower catalytic activity than that reduced at 300 °C as shown in Figure 1. For a clear comparison, the Pd 3d and In 3d XPS spectra of catalysts reduced at 300 and 400 °C are compared and presented in Figure 4C and Figure 4D, respectively. The XPS results show that Pd⁰ and In⁰ content increased and surface In/In₂O₃ ratio increased with the reduction temperature (Table 4). It has been reported that increasing the reduction temperature leads to the further reduction of In₂O₃ through the reaction of InPd + H₂ + In₂O₃ → Pd₂In₃ + H₂O.⁵² Thus, a higher reduction temperature (400 °C) results in the reduction of more In₂O₃ species and formation of In-rich Pd₂In₃ surfaces on catalyst 0.5%In₂O₃@Pd/MCF-400-H₂, which is consistent with STEM-EDS results and may lead to a low catalytic activity. These data suggested that an optimized structure of PdIn-In₂O₃ interface with suitable Pd/In and PdIn/In₂O₃ ratios is crucial for the activity of the catalysts for benzyl alcohol partial oxidation.

H₂ temperature programmed reduction (H₂-TPR) and time-resolved CO-DRIFT spectroscopy were performed to reveal the surface properties of In₂O₃ promoted Pd NPs catalysts. As known, the surface composition plays crucial role in the catalytic performance over a supported catalyst. H₂-TPR profiles of the catalysts yIn₂O₃@Pd/MCF-ox are displayed in Figure 5A. The reduction peak of PdO to Pd in

the range of 50 - 150 °C were observed on all $\gamma\text{-In}_2\text{O}_3@\text{Pd}/\text{MCF-ox}$ catalysts, indicating that surface PdO species was firstly reduced to Pd.⁵³ The small reduction peak on catalyst Pd/MCF-ox in the temperature range of 200 - 300 °C was commonly ascribed to the reduction of bulk PdO.⁵⁴ For sample 1.0% $\text{In}_2\text{O}_3/\text{MCF-ox}$, a weak reduction peak was observed in the temperature range of 300 - 400 °C, which is probably due to the reduction of highly dispersed In_2O_3 species⁵⁵ or this peak may arise from the formation of oxygen vacancies in the oxide.⁵⁶ As the temperature continue increasing up to 600 °C, the In_2O_3 gradually reduces to metallic In^{43,56}. For the PdIn NPs, it has been previously reported that the reduction peak in the range of 200 - 300 °C was due to the reduction of In_2O_3 near/on Pd nanoparticles thus forming Pd-rich PdIn intermetallic structure, while that in the range of 300 - 400 °C was ascribed to the reaction of PdIn with In_2O_3 to form In-rich intermetallic compound Pd_2In_3 on bimetallic PdIn NPs catalysts.⁵² In this work, the reduction peak in the temperature range of 200 - 400 °C was observed on all $\gamma\text{-In}_2\text{O}_3@\text{Pd}/\text{MCF-ox}$ catalysts. An enhancement of peak intensity was found with the increase of In_2O_3 content in the catalysts, suggesting that increased In_2O_3 content leads to the formation of more surface PdIn and/or Pd_2In_3 intermetallic structures. Another reduction peak in the range of 500 - 600 °C on $\gamma\text{-In}_2\text{O}_3@\text{Pd}/\text{MCF-ox}$ catalysts was attributed to further reduction of In_2O_3 on Pd_2In_3 with the formation of Pd_3In_7 ($\text{Pd}_2\text{In}_3 + \text{H}_2 + \text{In}_2\text{O}_3 \rightarrow \text{Pd}_3\text{In}_7 + \text{H}_2\text{O}$). Therefore, the reduction temperature of 300 °C is the junction point for the formation of Pd-rich PdIn intermetallic structure and In-rich Pd_2In_3 species. The catalytic activity was closely related to the reduction temperature, and catalyst

0.5%In₂O₃@Pd/MCF-300-H₂ reduced at 300 °C exhibits a higher catalytic activity than that reduced at 400 °C as shown in Figure 1. Therefore, we may conclude that the Pd-rich Pd_xIn_y intermetallic structure is more active for benzyl alcohol partial oxidation than the In-rich Pd_xIn_y.

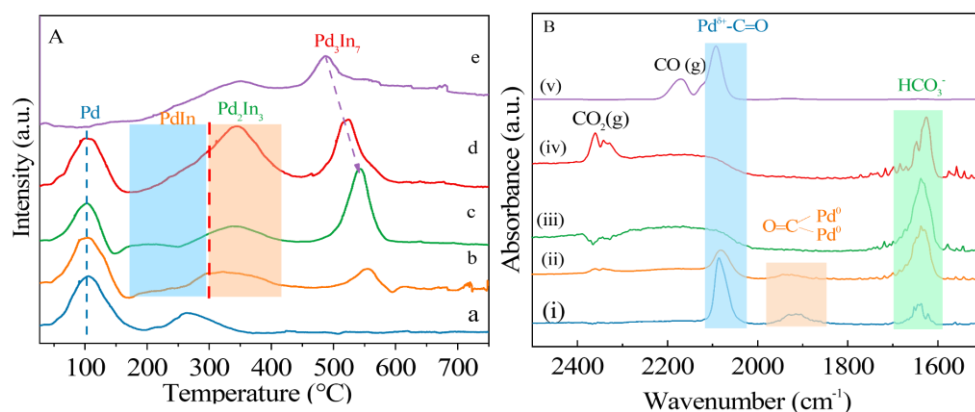


Figure 5. (A) H₂-TPR profiles of samples: (a) Pd/MCF-ox, (b) 0.2%In₂O₃@Pd/MCF-ox, (c) 0.5%In₂O₃@Pd/MCF-ox, (d) 1.0%In₂O₃@Pd/MCF-ox, and (e) 1.0%In₂O₃/MCF-ox and (B) DRIFT spectra of CO adsorbed on all catalysts: (i) Pd/MCF-300-H₂, (ii) 0.2% In₂O₃@Pd/MCF-300-H₂, (iii) 0.5%In₂O₃@Pd/MCF-300-H₂, (iv) 1.0% In₂O₃@Pd/MCF-300-H₂, (v) 0.5%In₂O₃@Pd/MCF-400-H₂.

The surface properties of In₂O₃ promoted Pd NPs catalysts yIn₂O₃@Pd/MCF-300-H₂ were characterized by time-resolved DRIFT using CO probe molecule and the results are shown in Figure 5B and Figure S5. The band at 2171 cm⁻¹ attributed to the adsorption of gaseous CO is present in all spectra.³² Two adsorption bands at 2096 and 1930 cm⁻¹ on catalysts Pd/MCF-300-H₂ and 0.2%In₂O₃@Pd/MCF-300-H₂ were observed associated with the linearly adsorbed CO on Pd^{δ+} located in the corner or edge sites of Pd nanoparticles^{57, 58} and bridge -

adsorbed CO molecules on contiguous Pd⁰ sites (ν_{CO} : 1900 - 2000 cm⁻¹),⁵⁹ respectively. These two peaks disappeared with increase of In₂O₃ content on catalysts 0.5%In₂O₃@Pd/MCF-300-H₂ and 1.0%In₂O₃@Pd/MCF-300-H₂. This result suggests a low exposure of surface Pd⁰ or Pd assemblies since CO is not adsorbed on metallic indium and indium oxide.^{30, 43} The absence of linear and bridge - adsorption peak of CO on catalysts 0.5%In₂O₃@Pd/MCF-300-H₂ and 1.0%In₂O₃@Pd/MCF-300-H₂ suggests that their surfaces are enriched in non-CO adsorbing indium species (metallic or oxide). Combining H₂-TPR and XPS results, it can be concluded that the formation of PdIn-In₂O₃ species only partially covered the Pd NPs on catalyst 0.2%In₂O₃@Pd/MCF-300-H₂, but fully covered the surface of Pd NPs on catalysts 0.5%In₂O₃@Pd/MCF-300-H₂ and 1.0%In₂O₃@Pd/MCF-300-H₂.³⁴ The band at 1633 cm⁻¹ attributed to the adsorbed HCO₃⁻ species³¹ and the band at 2350 cm⁻¹ corresponding to adsorbed CO₂³⁵ were observed on catalysts yIn₂O₃@Pd/MCF-300-H₂, which indicated that the introduction of In₂O₃ enhanced the surface oxidizing ability of bimetallic catalysts reduced at 300 °C. As the reduction temperature rises up to 400 °C, an obvious enhancement of linearly adsorbed CO band at 2091cm⁻¹ with a weak bridged CO adsorption band at 1931 cm⁻¹ were observed on catalyst 0.5%In₂O₃@Pd/MCF-400-H₂ indicating that more Pd species (mainly single Pd atoms) are exposed to CO adsorption after reduction at a higher temperature. However, nearly no HCO₃⁻ and CO₂ adsorption bands were detected for catalyst 0.5%In₂O₃@Pd/MCF-400-H₂, suggesting that the reduction of In₂O₃ and formation of In-rich PdIn intermetallic surface weakened the oxygen transfer ability

of the 0.5%In₂O₃@Pd/MCF-400-H₂ catalyst. Correlating the reaction results, it was found that a small amount of In₂O₃ can be used as an excellent oxygen transfer intermediate to improve the activation or transfer of O₂ in partial oxidation process, thus enhancing the catalytic activity of Pd NP catalyst on the 0.2%In₂O₃@Pd/MCF-300-H₂ catalyst. However, the active sites were covered or deactivated with excessive amount of In₂O₃ introduced in catalysts 0.5%In₂O₃@Pd/MCF-300-H₂ and 1.0%In₂O₃@Pd/MCF-300-H₂. Higher reduction temperature led to the formation of more linear adsorption sites but results in low catalytic activity, which suggests that the catalytic active sites for benzyl alcohol oxidation are not sole Pd atoms but Pd-rich PdIn species.

3.3 Catalyst' Chemistry. The reaction results indicated that catalyst 0.5%In₂O₃@Pd/MCF-300-H₂ prepared by *in situ* capture-alloying strategy exhibited higher catalytic activity than that prepared by wet-impregnation method. The recyclability of catalysts 0.5%In₂O₃@Pd/MCF-300-H₂ and 0.5%In₂O₃@Pd/MCF-im was evaluated in four consecutive reactions with repeated use of catalyst after regeneration, shown in Figure S7 and Table S3. As is shown in Figure S7 and Table S3, no obvious decrease of catalytic activity was observed on catalyst 0.5%In₂O₃@Pd/MCF-300-H₂ for 4 reaction cycles, while a continuous decrease of catalytic activity was detected on wet-impregnated catalyst 0.5%In₂O₃@Pd/MCF-im. HRTEM images shown in Figure 7S indicated a slight increase of noble metal NPs on both catalysts 0.5%In₂O₃@Pd/MCF-300-H₂ and 0.5%In₂O₃@Pd/MCF-im after 4 cycles, but ICP analysis revealed 30% of metal leaching from catalyst

0.5%In₂O₃@Pd/MCF-im while no leaching of Pd/In was observed on catalyst 0.5%In₂O₃@Pd/MCF-300-H₂. Both the reaction and characterization results revealed a good recyclability of catalyst 0.5%In₂O₃@Pd/MCF-300-H₂ prepared by *in situ* capture-alloying strategy, and a schematic illustration of PdIn-In₂O₃ interfaces construction was proposed and shown in Figure 6. Well-dispersed Pd NPs (1 ~ 3 nm) were immobilized in mesostructured cellular foam (MCF) silica through a one-pot synthesis process using MPTMS anchoring ligand. Indium species were introduced to the catalyst surface through a wet impregnation procedure. An in-situ capture-alloying process occurred during the H₂ reduction process (activation). Thus, the reduced In species were captured by the Pd NPs resulting in PdIn alloy NPs (1-4 nm), preventing the aggregation of In species during the activation process. The rational formation of PdIn-In₂O₃ interfaces was achieved with a low In loading (<0.5wt.%) and at an optimum reduction temperature of 300 °C, while further increasing reduction temperature (400 °C) led to the formation of In-rich PdIn alloy surfaces.

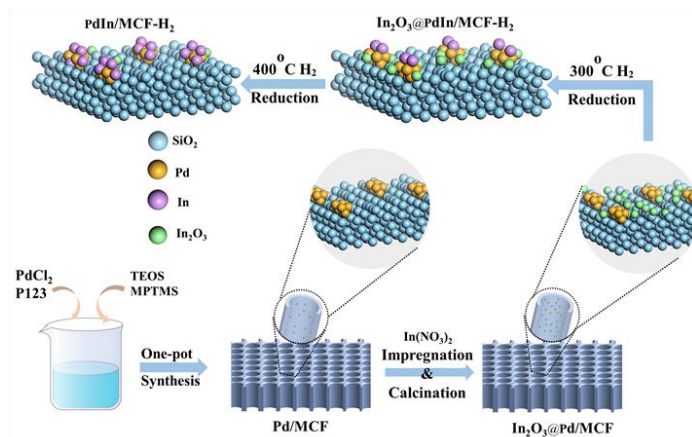


Figure 6. Formation of PdIn-In₂O₃ interfaces through capture-alloying strategy.

3.4 Reaction mechanism

The results presented (Figure 1 and Table S1-S2) indicated that the activity of catalysts is closely related to the reduction temperature and promoter content used. A relatively low In_2O_3 content (0.2wt.%) leads to a high catalytic activity of catalyst 0.2% In_2O_3 @Pd/MCF-300- H_2 , while further increase of In_2O_3 content (0.5wt.%) results in the decrease of activity with a high benzaldehyde selectivity (Table 1). A high In_2O_3 content (1.0wt.%) leads to both low catalytic activity and low benzaldehyde selectivity. As reported previously, metallic Pd^0 -enriched clusters/surface are active sites for O_2 activation.¹¹⁻¹⁶ XPS results indicate that the surface composition of these catalysts is PdIn- In_2O_3 /Pd assemblies and the coverage of Pd NPs was closely related to In_2O_3 content. Therefore, the high catalytic activity of the 0.2% In_2O_3 @Pd/MCF-300- H_2 catalyst was attributed to the exposure of more Pd-enriched surface, while relative high surface In_2O_3 content (0.5%) results in the formation of more surface PdIn- In_2O_3 species that may partially cover the active sites. These especially deactivate the active sites for deep oxidation, thus leading to decreased catalytic activity and increased benzaldehyde selectivity of catalyst 0.5% In_2O_3 @Pd/MCF-300- H_2 . Catalyst 0.5% In_2O_3 @Pd/MCF-300- H_2 reduced at 300 °C exhibits a higher catalytic activity than that reduced at 400 °C. H_2 -TPR data indicated the transformation of surface PdIn intermetallic species from Pd-rich Pd_xIn_y ($x>y$) to In-rich Pd_xIn_y ($x<y$) structures with the increase of reduction temperature from 300 °C to 400 °C. Correlating the catalytic results with the general characterization of catalysts, it is inferred that the coexistence of both PdIn- In_2O_3 interfaces and Pd assemblies led to high catalytic activity. The optimized

PdIn-In₂O₃/Pd ratio led to a high benzaldehyde selectivity, indicating that the catalytic activity and selectivity are derived from the variation of the PdIn-In₂O₃ interfaces. It was also observed that Pd-rich PdIn-species are more active for benzyl alcohol partial oxidation than the In-rich Pd₂In₃ species while the presence of PdIn-In₂O₃ interfaces facilitate the O₂ activation and O transfer. These findings were further justified by theoretical calculation.

The adsorption energies of benzyl alcohol, O₂ and benzaldehyde on Pd(111), Pd₃In₁(111), Pd₁In₃(111), In(101) and In₂O₃ surfaces, and energy barrier for the O₂ decomposition into 2O on different surfaces are obtained by theoretical calculations, as shown in Figure 7A and Table 5. The highest energy barrier for the O₂ decomposition was calculated on In₂O₃ surface (31.85 kcal/mol) because of the O saturation. Pd (111), Pd₁In₁(111) and In (101) surfaces exhibit similar O₂ decomposition energy barriers, around 7 ~ 8 kcal/mol. However, the formation of Pd-rich Pd₃In₁(111) surface facilitated the activation of oxygen molecules, and the decomposition energy barrier of O₂ to O atoms is reduced from 7 ~ 8 kcal/mol to 4.41 kcal/mol on the Pd₃In₁(111) surface. While the O₂ decomposition energy barrier increased obviously on In-rich Pd₁In₃(111) surface (17.05 kcal/mol), indicating the low oxygen activation ability of In-rich Pd₁In₃(111) surface. The Pd₃In₁(111)-In₂O₃ interface exhibited the lowest O₂ decomposition energy barrier (2.58 kcal/mol), indicating that the interface is most active for O₂ activation. On the other hand, a lower adsorption energy of benzaldehyde on Pd₃In₁(111) surface (-1.9 kcal/mol) than those on the surfaces of Pd (111) (-2.6 kcal/mol), Pd₁In₃(111) (-2.7 kcal/mol) and

In_2O_3 (-2.3 kcal/mol) was observed indicating the easy desorption of benzaldehyde from the $\text{Pd}_3\text{In}_1(111)$ surface. The results from the catalytic test confirmed that the Pd-rich $\text{PdIn-In}_2\text{O}_3$ interface is more active for benzyl alcohol partial oxidation than the In-rich Pd_2In_3 , which is theoretically confirmed by DFT calculation. The DFT results showed that the Pd-rich $\text{Pd}_3\text{In}_1(111)\text{-In}_2\text{O}_3$ interface facilitated the activation of oxygen molecules. A schematic illustration of catalytic mechanism over $\text{Pd-In-In}_2\text{O}_3$ interface of catalyst $\text{In}_2\text{O}_3@\text{Pd/MCF}$ was shown in Figure 7B. Both experimental and theoretical calculation results revealed that the Pd-rich $\text{PdIn-In}_2\text{O}_3$ interface is more active for benzyl alcohol partial oxidation. The DFT results (shown in Table 5) indicated that the Pd-rich sites facilitated the adsorption of benzyl alcohol, $\text{Pd}_3\text{In}_1(111)/\text{In}_2\text{O}_3$ interface facilitated the activation of oxygen molecules, and the low adsorption energy of benzaldehyde on $\text{Pd}_3\text{In}_1(111)$ surface leads to the easy desorption of benzaldehyde from Pd-rich surfaces, resulting in high catalytic activity and high benzaldehyde selectivity on Pd-rich $\text{PdIn-In}_2\text{O}_3$ interface.

Table 5. Adsorption Energies of Benzyl Alcohol/Oxygen/Benzaldehyde and Energy Barrier for the O_2 Decomposition into 2O on the Catalyst Surface

	$\text{C}_6\text{H}_5\text{CH}_2\text{OH}$ Ea (kcal/mol)	$\text{C}_6\text{H}_5\text{CHO}$ Ea (kcal/mol)	O_2 Ea (kcal/mol)	$\text{O}_2\text{-2O}$ Energy barrier Ea (kcal/mol)
Pd(111)	-2.88	-2.59	-0.75	8.01
$\text{Pd}_3\text{In}_1(111)$	-1.9	-1.9	-0.70	4.41
$\text{Pd}_1\text{In}_1(111)$	-1.79	-11.39	-0.74	7.56
$\text{Pd}_1\text{In}_3(111)$	-1.6	-2.7	-2.10	17.05
In(101)	-1.34	-1.23	-0.62	7.61
In_2O_3	-1.9	-2.3	-1.18	31.85
$\text{Pd}_3\text{In}_1(111)\text{In}_2\text{O}_3$				2.58

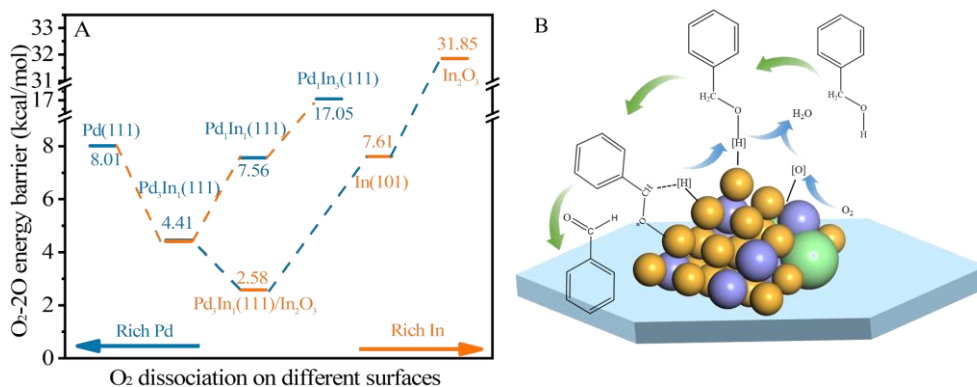


Figure 7. (A) Energy barrier for O₂ decomposition into 2O on different surface; (B) schematic illustration of catalytic mechanism over Pd-In-In₂O₃ interface of catalyst In₂O₃@Pd/MCF.

4. CONCLUSIONS

An *in situ* capture-alloying strategy was applied to prepare well-dispersed PdIn bimetallic alloy NPs (1 ~ 4 nm) on mesostructured silica support. A rational Pd-rich PdIn-In₂O₃ interface was constructed through changing the In₂O₃ loading and varying the reduction temperature. The performance of the catalysts for benzyl alcohol partial oxidation was evaluated and a catalytic synergy was observed. The catalytic performance was affected by both In₂O₃ loading and reduction temperature, which determined the surface composition. Catalyst 0.2%In₂O₃@Pd/MCF-300-H₂ with the low In₂O₃ amount reduced at 300 °C exhibited the highest catalytic activity (TOF=49400 h⁻¹). The Pd-rich PdIn-In₂O₃ interface is prone to formation on the catalyst reduced at 300 °C and/or with a low In₂O₃ content. The Pd-rich PdIn-In₂O₃

interface is more active for benzyl alcohol partial oxidation than In-rich PdIn species which is likely to form under a high reduction temperature (400 °C). The DFT results confirmed that the Pd-rich Pd₃In₁(111)-In₂O₃ interface facilitated the activation of oxygen molecules, leading to high catalytic activity. Considering that the design of metal/metal oxide promoted noble metal nanoparticle catalysts with highly efficient interfaces has been a long-standing challenge in nano-catalyst synthesis, the *in situ* capture-alloying strategy developed in this work provides a feasible way for active interface construction of promoted Pd nanoparticle catalysts, which could shed light on the rational design of high-performance catalysts with other noble metals for different catalytic reactions.

ASSOCIATED CONTENT

Supporting Information: N₂ adsorption/desorption isotherms; XRD spectra; STEM-EDS of reduced catalysts; HRTEM images, DRIFT spectra using CO probe molecule adsorbed on different catalysts, the time-resolved DRIFTS spectra collected on different catalysts at 25 °C under 1% CO in He (in the full range); recyclability of catalyst, benzyl alcohol oxidation results.

■ AUTHOR INFORMATION

Corresponding Authors

Peng Bai- *State Key Laboratory of Heavy Oil Processing, Key Laboratory of Catalysis, College of Chemical Engineering, China University of Petroleum (East China), Qingdao 266580, China;*

Email: baipeng@upc.edu.cn

Pingping Wu- *State Key Laboratory of Heavy Oil Processing, Key Laboratory of Catalysis, College of Chemical Engineering, China University of Petroleum (East China), Qingdao 266580, China;*

Email: wupp@upc.edu.cn

Lianming Zhao- *School of Materials Science and Engineering, Institute of Advanced Materials, China University of Petroleum (East China), Qingdao, 266580, China;*

Email: lmzhao@upc.edu.cn

Authors

Zhenxiang Zhao- *State Key Laboratory of Heavy Oil Processing, Key Laboratory of Catalysis, College of Chemical Engineering, China University of Petroleum (East China), Qingdao 266580, China;*

Yonghui Zhang- *State Key Laboratory of Heavy Oil Processing, Key Laboratory of Catalysis, College of Chemical Engineering, China University of Petroleum (East China), Qingdao 266580, China;*

Zhengke He- *State Key Laboratory of Heavy Oil Processing, Key Laboratory of Catalysis, College of Chemical Engineering, China University of Petroleum (East China), Qingdao 266580, China;*

Yonghui Liu- *School of Materials Science and Engineering, Institute of Advanced Materials, China University of Petroleum (East China), Qingdao, 266580, China;*

Chunzheng Wang- *State Key Laboratory of Heavy Oil Processing, Key Laboratory of Catalysis, College of Chemical Engineering, China University of Petroleum (East China), Qingdao 266580, China;*

Shixingwang Ma- *State Key Laboratory of Heavy Oil Processing, Key Laboratory of Catalysis, College of Chemical Engineering, China University of Petroleum (East China), Qingdao 266580, China;*

Svetlana Mintova- *Normandie University, ENSICAEN, UNICAEN, CNRS, Laboratoire Catalyse et Spectrochimie, 14000 Caen, France*

Zifeng Yan- *State Key Laboratory of Heavy Oil Processing, Key Laboratory of Catalysis, College of Chemical Engineering, China University of Petroleum (East China), Qingdao 266580, China;*

Notes

The authors declare no competing financial interest.

ACKNOWLEDGEMENTS

This work was financially supported by Shandong Provincial Natural Science Foundation (ZR2021ME020), Key Projects of Shandong Key R&D plan (2019JZZY010506), Taishan Scholar Foundation (tspd20210308), PetroChina

Research and Development Projects (2020A-1816, 2020A-1817) and the Sino-French International Laboratory (LIA) “Zeolites”.

REFERENCES

- (1) Li, L.; Jin, C.; Wang, X.; Ji, W.; Pan, Y.; van der Knaap, T.; van der Stoel, R.; Au, C. T., Cyclohexane Oxidation Over Size-Uniform Au Nanoparticles (SBA-15 hosted) in a Continuously Stirred Tank Reactor Under Mild Conditions. *Catal. Lett.* **2009**, *129* (3-4), 303-311.
- (2) Neumann, M.; Teschner, D.; Knop-Gericke, A.; Reschetilowski, W.; Armbrüster, M., Controlled Synthesis and Catalytic Properties of Supported In–Pd Intermetallic Compounds. *J. Catal.* **2016**, *340*, 49-59.
- (3) Pina, C. D.; Falletta, E.; Rossi, M., Highly Selective Oxidation of Benzyl Alcohol to Benzaldehyde Catalyzed by Bimetallic Gold–copper Catalyst. *J. Catal.* **2008**, *260* (2), 384-386.
- (4) Choudhary, V. R.; Dhar, A.; Jana, P.; Jha, R.; Uphade, B. S., A Green Process for Chlorine-free Benzaldehyde from the Solvent-free Oxidation of Benzyl Alcohol with Molecular Oxygen over a Supported Nano-size Gold Catalyst. *Green Chem.* **2005**, *7*, 768-770.
- (5) Chen, Y.; Guo, Z.; Chen, T.; Yang, Y., Surface-functionalized TUD-1 Mesoporous Molecular Sieve Supported Palladium for Solvent-free Aerobic Oxidation of Benzyl Alcohol. *J. Catal.* **2010**, *275* (1), 11-24.
- (6) McKenna, F.-M.; Wells, R. P.; Anderson, J. A., Enhanced Selectivity in Acetylene Hydrogenation by Ligand Modified Pd/TiO₂ Catalysts. *Chem. Commun.* **2011**, *47* (8), 2351-2353.
- (7) Zhou, C.; Chen, Y.; Guo, Z.; Wang, X.; Yang, Y., Promoted Aerobic Oxidation of Benzyl Alcohol on CNT Supported Platinum by Iron Oxide. *Chem. Commun.* **2011**, *47* (26), 7473-7475.
- (8) Haider, P.; Grunwaldt, J.-D.; Seidel, R.; Baiker, A., Gold Supported on Cu–Mg–Al and Cu–Ce Mixed Oxides: An in situ XANES Study on the State of Au during Aerobic Alcohol Oxidation. *J. Catal.* **2007**, *250* (2), 313-323.
- (9) Luo, M. F.; Hou, Z. Y.; Yuan, X. X.; Zheng, X. M., Characterization Study of CeO₂ Supported Pd Catalyst for Low-temperature Carbon Monoxide Oxidation. *Catal. Lett.* **1998**, *50* (3), 205-209.
- (10) Li, M.; Liu, R.; Han, G.; Tian, Y.; Xiao, Y., Facile Synthesis of Pd-Ni Nanoparticles on Reduced Graphene Oxide under Microwave Irradiation for Formic Acid Oxidation. *Chinese. J. Chem.* **2017**, *35*, 1405-1410..
- (11) Ghazal Tofghi, X. Y., Henning Lichtenberg, Dmitry E. Doronkin, Wu Wang, Christof Wöll, Yuemin Wang, and Jan-Dierk Grunwaldt, Chemical Nature of Microfluidically Synthesized AuPd Nanoalloys Supported on TiO₂. *ACS. Catal.* **2019**, *9* (6), 5462-5473.
- (12) Han, S.; Mullins, C. B., Surface Alloy Composition Controlled O₂ Activation on

Pd–Au Bimetallic Model Catalysts. *ACS. Catal.* **2018**, 8 (4), 3641-3649.

(13) Freakley, S. J.; He, Q.; Harrhy, J. H.; Lu, L.; Crole, D. A.; Morgan, D. J.; Ntainjua, E. N.; Edwards, J. K.; Carley, A. F.; Borisevich, A. Y.; Kiely, C. J.; Hutchings, G. J., Palladium-tin Catalysts for the Direct Synthesis of H₂O₂ with High Selectivity. *Science* **2016**, 351 (6276), 965-968.

(14) Wu, P.; Cao, Y.; Zhao, L.; Wang, Y.; He, Z.; Xing, W.; Bai, P.; Mintova, S.; Yan, Z., Formation of PdO on Au–Pd Bimetallic Catalysts and the Effect on Benzyl Alcohol Oxidation. *J. Catal.* **2019**, 375, 32-43.

(15) Xu, J. W., T.; Li, P.; He, C.; Yu, J.; Yuan, W.; Han, Y.-F., Biphase Pd–Au Alloy Catalyst for Low-Temperature CO Oxidation. *J. Am. Chem. Soc.* **2010**, 132, 10398-10406.

(16) Li, Z. G., F.; Furlong, O.; Tysoe, W. T., Adsorption of Carbon Monoxide Au/Pd (100) Alloys in Ultrahigh Vacuum: Identification of Adsorption Sites. *Surf. Sci.* **2010**, 604, 136-143.

(17) Hilaire, L. L. g., P.; Holl, Y.; Maire, G., Interaction of Oxygen and Hydrogen with Pd-Au Alloys: An AES and XPS Study. *Surf. Sci.* **1981**, 103, 125-140

(18) Adria R. Wilson, K. S., Miaofang Chi, Ryan M. White, James M. LeBeau, H. Henry Lamb and Benjamin J. Wiley, From Core–Shell to Alloys: The Preparation and Characterization of Solution-Synthesized AuPd Nanoparticle Catalysts. *J. Phys. Chem. C* **2013**, 117, 17557-17566.

(19) Wu, P.; He, Z.; Liu, Y.; Song, L.; Wang, C.; Muhumuza, E.; Bai, P.; Zhao, L.; Mintova, S.; Yan, Z., Compatibility between Activity and Selectivity in Catalytic Oxidation of Benzyl Alcohol with Au–Pd Nanoparticles through Redox Switching of SnO_x. *ACS Appl. Mater. Interfaces* **2021**, 13, 49780-49792.

(20) Xia, C.; Back, S.; Ringe, S.; Jiang, K.; Chen, F.; Sun, X.; Siahrostami, S.; Chan, K.; Wang, H., Confined Local Oxygen Gas Promotes Electrochemical Water Oxidation to Hydrogen Peroxide. *Nat. Catal.* **2020**, 3, 125-134.

(21) Zhang, Y.; Zhang, J.; Zhang, B.; Si, R.; Han, B.; Hong, F.; Niu, Y.; Sun, L.; Li, L.; Qiao, B., Boosting the Catalysis of Gold by O₂ Activation at Au-SiO₂ Interface. *Nat. Commun.* **2020**, 11 (1), 1-10.

(22) Peng, R.; Sun, X.; Li, S.; Chen, L.; Fu, M.; Wu, J.; Ye, D., Shape Effect of Pt/CeO₂ Catalysts on the Catalytic Oxidation of Toluene. *Chem. Eng. J.* **2016**, 306, 1234-1246.

(23) Wang, Y.; Deng, W.; Wang, Y.; Guo, L.; Ishihara, T., A Comparative study of the Catalytic Oxidation of Chlorobenzene and Toluene over Ce-Mn Oxides. *Mol. Catal.* **2018**, 459, 61-70.

(24) Valenti, M.; Prasad, N. P.; Kas, R.; Bohra, D.; Ma, M.; Balasubramanian, V.; Chu, L.; Gimenez, S.; Bisquert, J.; Dam, B., Suppressing H₂ Evolution and Promoting Selective CO₂ Electroreduction to CO at Low Overpotentials by Alloying Au with Pd. *ACS. Catal.* **2019**, 9 (4), 3527-3536.

(25) Zhu, X.; Guo, Q.; Sun, Y.; Chen, S.; Wang, J.-Q.; Wu, M.; Fu, W.; Tang, Y.; Duan, X.; Chen, D., Optimising Surface d Charge of AuPd Nanoalloy Catalysts for Enhanced Catalytic Activity. *Nat. Commun.* **2019**, 10 (1), 1-11.

(26) Chatterjee, S.; Griego, C.; Hart, J. L.; Li, Y.; Taheri, M. L.; Keith, J.; Snyder, J.

D., Free Standing Nanoporous Palladium Alloys as CO Poisoning Tolerant Electrocatalysts for the Electrochemical Reduction of CO₂ to Formate. *ACS. Catal.* **2019**, *9* (6), 5290-5301.

(27) Tian, P.; Xuan, F.; Ding, D.; Sun, Y.; Xu, X.; Li, W.; Si, R.; Xu, J.; Han, Y.-F., Revealing the Role of Tellurium in Palladium-tellurium Catalysts for the Direct Synthesis of Hydrogen Peroxide. *J. Catal.* **2020**, *385*, 21-29.

(28) He, Y.; Liang, L.; Liu, Y.; Feng, J.; Ma, C.; Li, D., Partial Hydrogenation of Acetylene using Highly Stable Dispersed Bimetallic Pd–Ga/MgO–Al₂O₃ Catalyst. *J. Catal.* **2014**, *309*, 166-173.

(29) Zhang, W.; Qin, Q.; Dai, L.; Qin, R.; Zhao, X.; Chen, X.; Ou, D.; Chen, J.; Chuong, T. T.; Wu, B., Electrochemical Reduction of Carbon Dioxide to Methanol on Hierarchical Pd/SnO₂ Nanosheets with Abundant Pd–O–Sn Interfaces. *Angew. Chem. Int. Edit.* **2018**, *57* (30), 9475-9479.

(30) Wu, Z.; E. C. W.; Tseng, H-T; Gallagher, J. R.; Harris, J. W.; Diaz, R. E.; Yang Ren, Ribeiro, F. H. and Miller, J. T. Pd-In Intermetallic Alloy Nanoparticles: Highly Selective Ethane Dehydrogenation Catalysts. *Catal. Sci. Technol.* **2016**, *6*, 6965-6976.

(31) Rameshan, C.; Lorenz, H.; Mayr, L.; Penner, S.; Zemlyanov, D.; Arrigo, R.; Haevecker, M.; Blume, R.; Knop-Gericke, A.; Schlögl, R., CO₂-selective Methanol Steam Reforming on In-doped Pd Studied by in situ X-ray Photoelectron Spectroscopy. *J. Catal.* **2012**, *295*, 186-194.

(32) Rui, N.; Wang, Z.; Sun, K.; Ye, J.; Ge, Q.; Liu, C.-j., CO₂ Hydrogenation to Methanol over Pd/In₂O₃: Effects of Pd and Oxygen Vacancy. *Appl. Catal. B-Environ.* **2017**, *218*, 488-497.

(33) Snider, J. L.; Streibel, V.; Hubert, M. A.; Choksi, T. S.; Valle, E.; Upham, D. C.; Schumann, J.; Duyar, M. S.; Gallo, A.; Abild-Pedersen, F., Revealing the Synergy between Oxide and Alloy Phases on the Performance of Bimetallic In–Pd Catalysts for CO₂ Hydrogenation to Methanol. *ACS. Catal.* **2019**, *9* (4), 3399-3412.

(34) Xiao, Y.; Xu, S.; Zhang, W.; Li, J.; Hu, C., One-Pot Chemo-Catalytic Conversion of Glucose to Methyl Lactate Over In/γ-Al₂O₃ Catalyst. *Catal. Today.* **2020**, *365*, 249-256.

(35) Du, Y.; Zhu, Y.; Xi, S.; Yang, P.; Moser, H. O.; Breese, M. B. H.; Borgna, A., XAFCA: a new XAFS Beamline for Catalysis Research. *J. Synchrotron. Rad.* **2015**, *22*, 839-843.

(36) Ravel, B.; Newville, M., ATHENA, ARTEMIS, HEPHAESTUS: Data Analysis for X-ray Absorption Spectroscopy using IFEFFIT. *J. Synchrotron. Rad.* **2005**, *12*, 537-541.

(37) Delley, B., An All - electron Numerical Method for Solving the Local Density Functional for Polyatomic Molecules. *J. Chem. Phys.* **1990**, *92* (1), 508-517.

(38) Delley, B., Fast Calculation Of Electrostatics in Crystals and Large Molecules. *J. Chem. Phys.* **1996**, *100* (15), 6107-6110.

(39) Perdew, J. P.; Burke, K.; Ernzerhof, M., Generalized Gradient Approximation Made Simple. *Phys. Rev. Lett.* **1996**, *77* (18), 3865-3868.

(40) Grimme, S., Semiempirical GGA - type Density Functional Constructed with a Long - Range Dispersion correction. *J. Comput. Chem.* **2006**, *27* (15), 1787-1799.

- (41) Zhao, L.; G., S.; Liu, H.; Zhu, H.; Yuan, S.; Guo, W., Density Functional Study of Hydrogen Evolution on Cobalt-Embedded Carbon Nanotubes: Effects of Doping and Surface Curvature. *ACS Appl. Nano Mater.* **2018**, *1*, 6258-6268.
- (42) Halgren, T. A.; Lipscomb, W. N., The Synchronous-transit Method for Determining Reaction Pathways and Locating Molecular Transition States. *Chem. Phys. Lett.* **1977**, *49* (2), 225-232.
- (43) Snider, J. L.; V. S.; Hubert, M. A.; Choksi, T. S.; Valle, E.; Upham, D. C.; Schumann, J.; Duyar, M. S.; Gallo, A.; Pedersen, F. A.;- T. F. J., Revealing the Synergy Between Oxide and Alloy Phases on the Performance of Bimetallic In–Pd Catalysts for CO₂ Hydrogenation to Methanol. *ACS Catal.* **2019**, *9*, 3399-3412.
- (44) Olmos, C. M.; Chinchilla, L. E.; Villa, A.; Delgado, J. J.; Hungría, A. B.; Blanco, G.; Prati, L.; Calvino, J. J.; Chen, X., Size, Nanostructure, and Composition Dependence of Bimetallic Au–Pd Supported on Ceria–Zirconia Mixed Oxide Catalysts for Selective Oxidation of Benzyl Alcohol. *J. Catal.* **2019**, *375*, 44-55.
- (45) Teranishi, T.; Miyake, M., Size Control of Palladium Nanoparticles and Their Crystal Structures. *Chem. Mater.* **1998**, *10* (2), 594-600.
- (46) Farrauto, R. J.; Lampert, J. K.; Hobson, M. C.; Waterman, E. M., Thermal Decomposition and Reforming of PdO Catalysts; Support Effects. *Appl. Catal. B-Environ.* **1995**, *6* (3), 263-270.
- (47) Wang, H.; Wang, C.; Yan, H.; Yi, H.; Lu, J., Precisely-controlled Synthesis of Au@Pd Core-shell Bimetallic Catalyst via Atomic Layer Deposition for Selective Oxidation of Benzyl Alcohol. *J. Catal.* **2015**, *324*, 59-68.
- (48) Weerachawanasak, P.; Hutchings, G. J.; Edwards, J. K.; Kondrat, S. A.; Miedziak, P. J.; Prasertham, P.; Panpranot, J., Surface Functionalized TiO₂ Supported Pd Catalysts for Solvent-free Selective Oxidation of Benzyl Alcohol. *Catal. Today.* **2015**, *250*, 218-225.
- (49) Jiang, T.; Jia, C.; Zhang, L.; He, S.; Sang, Y.; Li, H.; Li, Y.; Xu, X.; Liu, H., Gold and Gold-palladium Alloy Nanoparticles on Heterostructured TiO₂ Nanobelts as Plasmonic Photocatalysts for Benzyl Alcohol Oxidation. *Nanoscale* **2015**, *7* (1), 209-217.
- (50) Detweiler, Z. M.; White, J. L.; Bernasek, S. L.; Bocarsly, A. B., Anodized Indium Metal Electrodes for Enhanced Carbon Dioxide Reduction in Aqueous Electrolyte. *Langmuir* **2014**, *30* (25), 7593-7600.
- (51) Chen, M. X.; Liu, Y. M.; Cao, Y.; He, H. Y.; Zhuang, J. H., Supported Indium Oxide as Novel Efficient Catalysts for Dehydrogenation of Propane with Carbon Dioxide. *Appl. Catal. A-GEN.* **2010**, *377*, 35-41.
- (52) Neumann, M. T. D.; Knop-Gericke, A.; Reschetilowski, W.; Armbrüster, M., Controlled Synthesis and Catalytic Properties of Supported In-Pd Intermetallic Compounds. *J. Catal.* **2016**, *340*, 49-59.
- (53) Markov, P.; Bragina, G.; Baeva, G.; Tkachenko, O.; Mashkovskii, I.; Yakushev, I.; Vargaftik, M.; Stakheev, A. Y., Supported Catalysts Based on Pd–In Nanoparticles for the Liquid-phase Hydrogenation of Terminal and Internal Alkynes: 1. Formation and Structure. *Kinet. Catal.* **2016**, *57* (5), 617-624.
- (54) Hosseini, M.; Barakat, T.; Cousin, R.; Aboukaïs, A.; Su, B.-L.; De Weireld, G.;

Siffert, S., Catalytic Performance of Core-shell and Alloy Pd–Au Nanoparticles for Total Oxidation of VOC: The Effect of Metal Deposition. *Appl. Catal. B-Environ.* **2012**, *111*, 218-224.

(55) Marchesini, F.; Gutierrez, L.; Querini, C.; Miró, E., Pt, In and Pd, In Catalysts for the Hydrogenation of Nitrates and Nitrites in Water. FTIR Characterization and Reaction Studies. *Chem. Eng. J.* **2010**, *159* (1-3), 203-211.

(56) Martin, O.; Martín, A. J.; Mondelli, C.; Mitchell, S.; Segawa, T. F.; Hauert, R.; Drouilly, C.; Curulla - Ferré, D.; Pérez - Ramírez, J., Indium Oxide as a Superior Catalyst for Methanol Synthesis by CO₂ Hydrogenation. *Angew. Chem. Int. Edit.* **2016**, *55* (21), 6261-6265.

(57) Dai, Q.; Zhu, Q.; Lou, Y.; Wang, X., Role of Brønsted acid Site during Catalytic Combustion of Methane over PdO/ZSM-5: Dominant or Negligible? *J. catal.* **2018**, *357*, 29-40.

(58) Yu, W.-Y.; Mullen, G. M.; Mullins, C. B., Hydrogen Adsorption and Absorption with Pd–Au Bimetallic Surfaces. *J. Phys. Chem. C.* **2013**, *117* (38), 19535-19543.

(59) Yang, G.; Frenkel, A. I.; Su, D.; Teng, X., Enhanced Electrokinetics of C–C Bond Splitting during Ethanol Oxidation by Using a Pt/Rh/Sn catalyst with a Partially Oxidized Pt and Rh Core and a SnO₂ Shell. *ChemCatChem* **2016**, *8* (18), 2876-2880.

Graphic for manuscript

